VISCOUS FLOW IN A POROUS CHANNEL WITH STRETCHING AND SHRINKING WALLS

Aamir ALI[1], Dil Nawaz KHAN MARWAT[2], Sagheer Ahmad SHAH[3]

In this paper Berman's problem is modified by considering different porosities and stretching/shrinking velocities at walls of the channel. The upper (lower) wall has porous velocity $v_w\left(u_w\right)$ *and upper (lower) wall is stretched / shrunk with the velocity* $Ax\left(Bx\right)$ *where* $A>0\left(<0\right)$, $B>0\left(<0\right)$ *are the stretching (shrinking) constants for the upper and lower plate, respectively and* x *is the axial coordinate. The governing PDE's with no slip conditions are simplified and converted into boundary value ODE's. Analytical solutions of the final problem are obtained by using perturbation and asymptotic methods for small and large values of the Reynolds number, respectively. For a range of parameter values, an exact solution of the governing Navier-Stokes equation is also provided. Multiple solutions are also presented for a single set of parameter values. The two analytical and exact solutions are compared with the results given by the numerical method. Berman's results are recovered for* $A=B=0$ *and* $v_w=-u_w$.

Keywords: Porous walls; stretched (shrunk); channel flow; asymptotic solution.

1. Introduction

In processes of extrusion and melt-spinning, the fluid motion is mostly generated (near the material being extruded) by the moving surfaces. The same phenomenon is also observed during the manufacturing of plastic and rubber sheets. Further, stretching (shrinking) surfaces are using for blowing of a gaseous medium through the material. The flow due to moving surfaces is also used for the cleaning of a large metallic plate in bath. The fluid flow induced by the shrinking (stretching) of the plates has applications in glass blowing, continuous casting and the spinning of fibers. The first study on the boundary-layer adjacent to a continuous moving surface was conducted by [1] and later on this model is generalized and refined. The Falkner Skane flow models over a stretching sheet

[1] Dept. of Mathematics, COMSATS University Islamabad, Attock Campus, Attock Pakistan, e-mail: aamir_ali@cuiatk.edu.pk
[2] Dept. of Mathematics, Faculty of Engineering and Technology, Islamia College Peshawar, Pakistan, e-mail: dilnawazkhan@ico.edu.pk
[3] Dept. of Mathematics, University of Science and Technology Bannu Pakistan,, e-mail: 9797322@gmail.com

for a viscous fluid were examined by [2], with the boundary-layer approximations. A flow model corresponding to two-dimensional flows in a porous channel is developed by [3]. The governing equations are simplified by introducing proper similarity transformation and solved by perturbation method for small cross flow Reynolds number. Later on the Berman problem is solved for large suction Reynolds (high injection Reynolds) number see [4].

The Berman problem is extended for uniform suction (injection) through the upper wall, the lower wall being considered impermeable see [5]. They discussed the similarity and steady state solutions numerically. The asymptotic solutions are discussed in the limits of small wall suction (injection), large wall injection (suction). Channel flow due to non-uniform suction (injection) through its uniformly porous parallel walls is studied by [6]. The solutions are valid for large suction (injection) velocities. The governing equations obtained after similarity transformation are solved using the series method with polynomial coefficients. Two different solutions of the Berman's problem are investigated, one corresponding to injection and the other one to suction. They compared the asymptotic and numerical results and found excellent agreement between them. The viscous flow between a corrugated wall and the first liquid layer using slip conditions is studied by [15]. They examined the periodic roughness on the slip length which spans multiple length scales ranging from molecular to macroscopic dimensions. The Berman's problem with accelerating rigid porous walls is studied by [7]. The upper wall of the channel is considered porous and having a uniform stretching velocity. They discussed the existence of multiple solutions and found conditions for exponential terms in matched asymptotic expansion. The analytical predictions were verified by numerical results.

Recently the flow problem between parallel, porous and deforming walls see [8] was solved by the homotopy analysis and homotopy perturbation methods for small deformation rate and the results are confirmed by non-linear shooting method in [9]. A model of mixed convective viscous fluid flow in a vertical microchannel having parallel, porous and deforming walls is examined by [10]. Experimental study of transpiration cooling due to motion of heated fluid in vertical parallel and porous plates is provided by [11]. The study is further extended to hydromagnetic flow and heat transfer in a porous channel. The effects of non-Darcy porous medium with convective cooling of the wall have been analyzed by [12]. Effects of MHD flow on micropolar nanofluid flow inside a porous channel with uniform injection have been presented by [13]. [14] studied the heat transfer in a micropolar fluid over a porous channel and the results are obtained by Akbari-Ganji's Method (AGM).

In this paper a generalized form of Berman's problem is investigated. The sources considered here are: (i) the porous velocity at the upper wall, denoted by v_w, and that at the lower wall, denoted by u_w, are not equal (ii) the upper (lower)

wall is stretched (shrunk) with velocity $Ax\,(Bx)$ where $A>0(<0)$, $B>0(<0)$ are the stretching (shrinking) constants for the upper and lower plate, respectively and x is the axial coordinate. The problem is formulated as governing equations and special boundary conditions. The PDE's are converted into ODE's by using the similarity transformation. The solution of the non-dimensional ODE with four boundary conditions is obtained by perturbation method for small values of the parameters and asymptotic method for large values of the parameters. The correctness of these two solutions is presented by a powerful numerical technique given by [15]. The results obtained by the perturbation method and the numerical method are compared. In most cases there is no error between the two solutions up to five decimal places. Similarly, the asymptotic results are compared with numerical results and excellent agreement between the two is found. Those values of the unknown functions are taking into account in which error is significant. To the best of author's knowledge, the idea presented in this paper has not been discussed so far. Flows in a channel induced by different porosity at walls and non-uniform stretching (shrinking) walls are known to have important relevance for fluid transport in many biological and engineering systems. It is thus hoped that the study may add some mathematical features to this important biological and engineering problems. The classical Berman's problem is a special case of the current study.

2. Formulation of the Problem

Let us investigate the flow of viscous fluid in a two-dimensional channel. The gap between the wall is $2h$. Both walls of the channel are porous and have different permeabilities. Each wall has its own stretching (shrinking) velocity. A rectangular coordinate system is selected in such a way that x and y-axes lie along and normal to the center line, respectively. The longitudinal and transversal velocity components are denoted by u and v. The channel geometry is described in Figure 1.

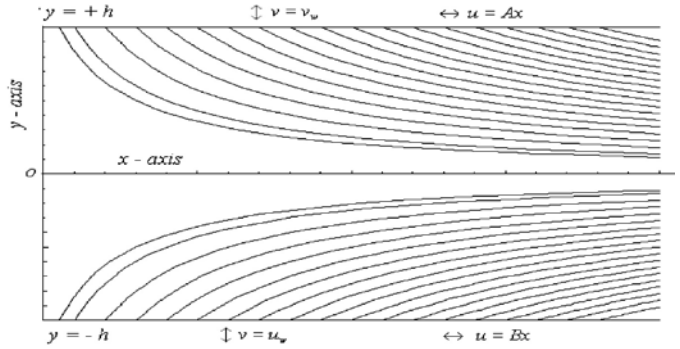

Fig. 1: Geometry of converging (diverging) channel under consideration

The governing equations are composed of the continuity and Navier Stokes equations as follow:

$$\frac{\partial u}{\partial x}+\frac{1}{h}\frac{\partial v}{\partial \eta}=0, \tag{1}$$

$$u\frac{\partial u}{\partial x}+\frac{v}{h}\frac{\partial u}{\partial \eta}=-\frac{1}{\rho}\frac{\partial p}{\partial x}+\upsilon[\frac{\partial^2 u}{\partial x^2}+\frac{1}{h^2}\frac{\partial^2 u}{\partial \eta^2}], \tag{2}$$

$$u\frac{\partial v}{\partial x}+\frac{v}{h}\frac{\partial v}{\partial \eta}=-\frac{1}{h\rho}\frac{\partial p}{\partial \eta}+\upsilon[\frac{\partial^2 v}{\partial x^2}+\frac{1}{h^2}\frac{\partial^2 v}{\partial \eta^2}], \tag{3}$$

in which $\eta = y/h$, is the dimensionless similarity variable, p is the pressure, ρ is the constant and uniform fluid density and υ is the kinematic viscosity. The governing equations are only valid for laminar and incompressible flow in the rectangular domain bounded by the two parallel permeable and stretching (shrinking) surfaces. The appropriate boundary conditions are:

$$u(x,1)=Ax,\ u(x,-1)=Bx,\ v(x,1)=v_w,\ v(x,-1)=u_w, \tag{4}$$

where Ax and Bx represent the stretching (shrinking) velocities of the upper and lower wall respectively. Here, $A \succ 0$ and $B \succ 0$ correspond to stretching walls, while $A \prec 0$ and $B \prec 0$ refer to shrinking walls. Similarly, v_w and u_w are the injection (suction) velocities at the upper and lower wall, respectively. For two-dimensional incompressible flows a stream function ψ exists which satisfy the continuity Eq. (1) automatically such that the velocity v_w at the upper wall and the given boundary condition gives a possible choice for the stream function:

$$u(x,\eta)=\frac{1}{h}\frac{\partial \psi}{\partial \eta},\ v(x,\eta)=-\frac{\partial \psi}{\partial x}\ \text{where}\ \psi(x,\eta)=-v_w x f(\eta). \tag{5}$$

The governing equations in a channel with porous and stretching (shrinking) walls are simplified by using a proper procedure. The velocities are different at the walls, and the walls are stretching (shrinking) with different velocities. The stream function in Eq. (6) may lead to an exact similarity solution of the Navier-Stokes equations in rectangular channel with porous and stretching walls. In view of Eq. (6), the velocity components emerge as:

$$u(x,\eta)=-v_w x h^{-1} f'(\eta),\ v(x,\eta)=v_w f(\eta), \tag{6}$$

by substituting the expressions for u and v given in Eq. (6) into Eqs. (2-3) we get:

$$f'^2 - ff'' = -\frac{h^2}{\rho x v_w^2}\frac{\partial p}{\partial x} - \frac{1}{\mathrm{Re}} f''' \text{ and } \frac{v_w^2}{h} ff' = -\frac{1}{\rho h}\frac{\partial p}{\partial \eta} + \frac{\upsilon}{h^2} v_w f'', \tag{7}$$

where $\mathrm{Re} = hv_w / \upsilon$ is the Reynolds number. Eliminating pressure from Eq. (7):

$$\mathrm{Re}\left(ff'' - ff'''\right) = -f^{(iv)} \text{ or } \left(f'^2 - ff''\right) + \varepsilon f''' = k. \tag{8}$$

The first part in Eq. (8) is divided by Re and integrating w. r. t η we get the second part of it. Where $\varepsilon = 1/\mathrm{Re}$ and k is a subsidiary constant of integration. The BC's (4) are converted for $f(\eta)$ as under:

$$f(1) = 1,\ f'(1) = \alpha_1,\ f'(-1) = \alpha_2,\ f(-1) = d, \tag{9}$$

where $\alpha_1 = -Ah / v_w,\ \alpha_2 = -Bh / v_w,\ d = u_w / v_w.$

The normal and axial pressures are calculated form Eq. (7) as:

$$\frac{\partial p}{\partial x} = \frac{k_1 x \mu v_w}{h^2},\ \frac{\partial p}{\partial y} = \frac{\mu}{h} v_w f'' - \rho v_w^2 ff', \tag{10}$$

where k_1 is a constant of integration appeared in Eq. (8) and μ is the absolute viscosity. The Eq. (10) is simply obtained by using Eq. (8) in Eq. (7). The shear stress is obtained as:

$$\tau_{xy} = \mu\left(\frac{\partial u}{\partial y} + \frac{\partial v}{\partial x}\right) = \tau_w f''(\eta), \tag{11}$$

with $u(x,\eta)$ from Eq. (6), we get: $\tau_w = -x\mu v_w / h^3$. The parameter values subject to certain range have the physical meanings. For $\alpha_1 = 0\ (\alpha_2 = 0)$, $\alpha_1 > 0\ (\alpha_2 > 0)$ and $\alpha_1 < 0\ (\alpha_2 < 0)$, the upper (lower) wall is fixed, stretching and shrinking, respectively. Similarly for equal suction (injection) at both walls we have $d = -1$ and $\mathrm{Re} < 0\ (> 0)$ whereas for equal top suction (injection) and lower injection (suction), the parameters ranges are: $d = 1$ and $\mathrm{Re} < 0\ (> 0)$. Moreover, for $d < -1$ and $\mathrm{Re} < 0\ (> 0)$, the top suction (injection) is smaller than lower suction (injection) and for $d > 1$ and $\mathrm{Re} < 0\ (> 0)$ the top suction (injection) is greater (smaller) than the lower injection (suction). On the other hand, for $-1 < d < 0$ and $\mathrm{Re} < 0\ (> 0)$, lower injection (suction) is smaller than top injection (suction) and for $0 < d < -1$ and $\mathrm{Re} < 0\ (> 0)$, the lower injection (suction) is smaller than top suction (injection). Finally, for

$d = 0$ and $\mathrm{Re} < 0\ (> 0)$, the lower wall is rigid (non-porous) and injection (suction) is taking place in top wall. The ODE's to be solved is Eq. (8) together with the associated boundary conditions (9). This constitutes an exact similar problem for the governing equations.

3. Solution to the Problem

Solution of Eq. (8) satisfying the boundary conditions in Eq. (9) is attempted by three different methods. The first one is the numerical method developed by [15], the second and third methods are the perturbation and asymptotic methods, respectively. The perturbation results are accurate for small values of the parameters and the asymptotic results are valid for large values of the parameters. The asymptotic results are also checked for small values of the parameters. The zeroth order perturbation solution is obtained when we put $\mathrm{Re} = 0$ in Eq. (8). Note that the order of equation is not changed by the substitution while the nonlinear terms in the equation are eliminated. This approximation (technique) can help us in simplifying the boundary value ODE in Eq. (8). The function f can be easily obtained from the Eqs. (8, 9) by this method. An approximate solution of Eqs. (8-9) is investigated for large value of Re. In Eq. (8) $\mathrm{Re} = 1/\varepsilon$, and large Re means small ε. The order of the equation is reduces by unity if the terms do not have Re as a factor. Thus, we obtained a solution to the unmodified equation for large Re.

3.1. Perturbation solution for small Re

Here we investigate the perturbation solution of the boundary value ODE in Eq. (8, 9) for small values of the Reynolds number. Expanding the solution $f(\eta)$ of Eq. (8) in terms of Re, where Re is assumed a small quantity:

$$f(\eta) = f_0(\eta) + \mathrm{Re}\, f_1(\eta) + O(\mathrm{Re}^2). \tag{12}$$

Here the unknown functions f_0, f_1 are taken to be independent of Re. Substituting (12) into Eqs. (8,9) and collecting like powers of Re leads to the zeroth and first order equations in Re. The zeroth and first order boundary value ODE's in Re have the following solutions.

$$f_0 = A_0 + A_1\eta + A_2\eta^2 + A_3\eta^3, \tag{13}$$

$$f_1 = B_0 + B_1\eta + B_2\eta^2 + B_3\eta^3 + B_4\eta^4 + B_5\eta^5 + B_6\eta^6 + B_7\eta^7, \tag{14}$$

where $A_0 = (2 + 2d - \alpha_1 + \alpha_2)/4$, $A_1 = (3 - 3d - \alpha_1 - \alpha_2)/4$, $A_2 = (\alpha_1 - \alpha_2)/4$, $A_3 = (-1 + d + \alpha_1 + \alpha_2)/4$, $B_0 = (-5A_1A_2 + 15A_0A_3 - 4A_2A_3)/60$, $B_1 = (-7A_2^2 - 6A_3^2)/210$, $B_2 = (5A_1A_2 - 15A_0A_3 + 3A_2A_3)/30$,

$B_3 = (14A_2^2 + 9A_2^3)/210,\ B_4 = (-A_1A_2 + 3A_0A_3)/12,\ B_5 = -A_2^2/30,\ B_6 = -A_2A_3/30$ and $B_7 = -A_3^2/70.$ The final perturbation solution can be obtained by substituting the expressions for f_0 in Eq. (13), f_1 in Eq. (14) into Eq. (12). We get:

$$f(\eta) = (A_0 + A_1\eta + A_2\eta^2 + A_3\eta^3) + \mathrm{Re}(B_0 + B_1\eta + B_2\eta^2 + B_3\eta^3 + B_4\eta^4 + B_5\eta^5 + B_6\eta^6 + B_7\eta^7) + O(\mathrm{Re}^2). \tag{15}$$

3.2. Asymptotic solution for large Re

Asymptotic solution for large values of Re is also presented here. This solution will satisfy some conditions on the parameters values. Only zeroth order solution is obtained and this solution is valid for wide range of parameters values. Moreover, the parameters α_1 and α_2 are depending on d. We expand the function f and constant k of Eq. (12) in terms of ε as:

$$f = f_0 + O(\varepsilon),\ k = k_0 + O(\varepsilon), \tag{16}$$

where the unknown functions f_0, f_1 are no longer dependent on ε. Substituting assumptions (16) for f and k into Eqs. (8-9) and collecting like powers of ε:

$$(f_0'^2 - f_0 f_0'') = k_0,\quad f_0(1) = 1,\ f_0'(1) = \alpha_1,\quad f_0'(-1) = \alpha_2,\ f_0(-1) = d, \tag{17}$$

and solution of Eq. (17) is:

$$f_0 = g_1\cos(\bar{\eta}) + g_2\sin(\bar{\eta}), \tag{18}$$

where $\alpha_1 = (1-2d)\pi/\varepsilon,\quad \alpha_2 = (2-d)\pi/(\sqrt{3}\varepsilon),\quad g_1 = d,\quad g_2 = (2-d)/\sqrt{3},$ $k_0 = \pi^2\left(g_1^2 + g_2^2\right)/36$ and $\bar{\eta} = \pi(\eta+1)/\varepsilon.$ Note that the solution in Eq. (18) is valid for special values of α_1, α_2 and dependent on parameter d.

3.3. Exact solution

The Eqs. (11, 13) has the exact solution when $\alpha_1 = \alpha_2$ and $d + 2\alpha_1 = 1$:

$$f(\eta) = A_0 + A_1\eta \tag{19}$$

where $A_0 = (1+d)/2$ and $A_1 = (1-d)/2.$ The linear exact solution in Eq. (19) is confirmed by the perturbation solution in Eq. (15) and numerical method. This solution is independent of Re. The profiles are shown in different graphs by straight lines. Further, for $d = 1,$ the exact solution is converted into a constant solution and the constant has the value one.

3.4. Multiple solution

Multiple solutions of Eqs. (8, 9) are found by the modified shooting method and the scheme is developed by [15]. Note that the method requires initial guess for calculating the solution of any boundary value problem. Here we consider only one case and assumed fixed values for the parameter $\mathrm{Re} = 5, \alpha_1 = \alpha_2 = 0$ and $d = -1.6$. For this set of parameters values, we obtained three multiple solutions as shown in Fig 7. For $-1 \le d \le 0$, the initial guess has no impact on the profiles. This means that the profiles are exactly the same for every choice of the initial guess. For $d < -1$, the solution is strongly initial guess dependent. For that choices of d, we may obtain multiple solutions. The cheep solution which is obtained easily for this set of parameters values and presented in Fig. 2 by pattern A. The solution in pattern B can be matched with the perturbation solution. The solution in pattern A and C cannot be obtained from perturbation solutions. All the patterns are uniformly changed with changing the values of d for special values of initial guesses given in the legends of the figure.

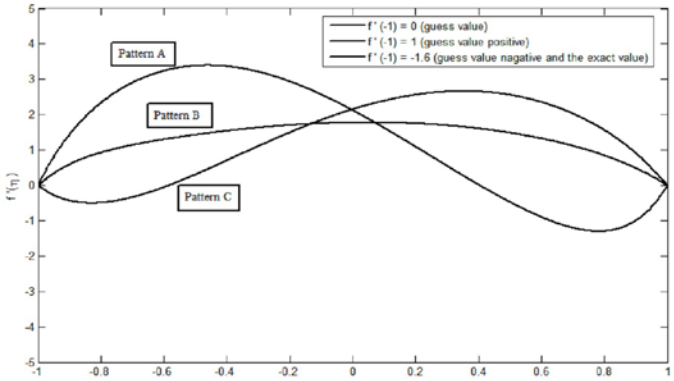

Fig. 2: Multiple solutions for $f'(\eta)$ are plotted against η for $\alpha_1 = \alpha_2 = 0$ and $\mathrm{Re} = 5$, $d = -1.6$.

3.5. Comparison of analytical and numerical solutions

The perturbation solution in Eq. (15) is compared with the numerical solution of Eqs. (8, 9). These two solutions are compared for certain range of parameters values and matched. The perturbation results presented for the sake comparison are accurate up to $O(\mathrm{Re}^6)$. The two solutions agreed to reasonable order of accuracy level. It is observe that for all sets of parameters values there are no differences between two solutions near walls and center of the channel. The solution in Eq. (17) is compared with numerical solutions of Eqs. (8, 9) for large values of parameters d, Re and compared the results. In most cases the results obtained by these two methods are exactly the same. Again the solution in Eq. (17) is compared with the numerical solution of Eqs. (8, 9) for small value of

d and Re in Table 1 and good agreement between the two is found. Although the solution in Eq. (17) is obtained for large values of the parameters but it also provides accurate results for small values of the parameters.

Table 1:

Comparison of asymptotic and numerical solutions for large d and Re.

η	Numeric (f_n)	Analytic (f_a)	Error $\lvert f_n - f_a \rvert$	η	Numeric (f_n)	Analytic (f_a)	Error $\lvert f_n - f_a \rvert$
$\mathrm{Re}=5,\ d=-1,\ \alpha_1=\alpha_2=0.9069$				$\mathrm{Re}=-5,\ d=1,\ \alpha_1=\alpha_2=0.3023$			
-0.9697	-0.9724	-0.9724	0.0000	-0.9798	1.0060	1.0061	0.0001
-0.8384	-0.8499	-0.8500	0.0001	-0.8586	1.0397	1.0400	0.0003
-0.7374	-0.7529	-0.7531	0.0002	-0.7980	1.0548	1.0554	0.0006
-0.6364	-0.6538	-0.6541	0.0003	-0.7172	1.0733	1.0742	0.0009
-0.6162	-0.6338	-0.6341	0.0003	-0.6364	1.0900	1.0912	0.0012
-0.1919	-0.2004	-0.2006	0.0002	-0.5758	1.1012	1.1026	0.0014
-0.1111	-0.1162	-0.1163	0.0001	-0.4747	1.1174	1.1192	0.0018
0.0000	0.0000	0.0000	0.0000	-0.3131	1.3272	1.3292	0.0020
0.0707	0.0739	0.0740	0.0001	-0.0707	1.1519	1.1539	0.0020
0.1717	0.1794	0.1796	0.0002	0.0909	1.1516	1.1534	0.0018
0.1818	0.1899	0.1901	0.0002	0.2525	1.1432	1.1446	0.0014
0.3232	0.3366	0.3369	0.0003	0.3535	1.1338	1.1350	0.0012
0.7576	0.7725	0.7727	0.0002	0.4545	1.1212	1.1222	0.0010
0.8485	0.8595	0.8596	0.0001	0.7374	1.0694	1.0697	0.0003
0.9697	0.9724	0.9724	0.0000	0.9798	1.0060	1.0061	0.0001

4. Results and Discussions

The governing PDE's and boundary conditions are converted into boundary value ODE by well established similarity transformations. As a result, Eqs. (8, 9) are formed and solved by perturbation method for small values of Re. The perturbation solution is shown in Eq. (15) and valid up to $O(\mathrm{Re}^2)$. The problem is also solved by the asymptotic method for large values of Re. The solution is shown in Eq. (17). Note that the asymptotic solution is valid until and unless, the parameters will fulfill a certain criteria and further conditions are used for parameter values. For a set of parameter values, the exact solution to the

problem is provided and the solution is independent of Re. The validity of the two analytical solutions i.e. solution for small and large values of the parameters and exact solution is also shown by a powerful numerical scheme developed by [15]. Some highlights of the solutions for special values of emerging parameters are discussed in details. Different cases are discussed and presented here. In Fig. 3, effects of different $\mathrm{Re} = 20, 10, 5, 0, -5, -10, -20$, $\alpha_1 = 0 = \alpha_2$ and $d = -1$ are observed on the axial velocity component f'. This is the case of well-known Berman's problem [3] when $\alpha_1 = 0$ and $d = -1$ i.e. both the equation and boundary conditions in Eqs. (8, 9) are reduced to that of Berman Problem. For these special values of the parameters, the perturbation solution in Eq. (15) is reduced to the solution of [3]. It is observed that the shapes of f' are changed smoothly over the wide range of Re. In case of equal suction ($\mathrm{Re} > 0$) at both walls, the profiles corresponding to large suction are flatten and inclined toward the walls. The same profiles for large injection have high peaks and escaping from the walls. For large and positive values of Re the profiles are steeper and mounted with small peaks. On the other hand for large negative values of Re the profiles have highest peaks and slowest steep. Moreover, the profiles are symmetrical about the centre line for all values of Re. For large values of Re the solution is similar to that of [4] obtained for [3]. In Fig. 4, f' is plotted against the similarity variable η for the combination of equal suction (injection) at upper and lower walls with shrinking parameters ($\alpha_1 < 0$ and $\alpha_2 < 0$). The profiles are symmetrical about midway. For moderate values of suction and shrinking parameters, the profiles have high peaks. For large suction and equal shrinking ($\alpha_1 = \alpha_2 < 0$), flat profiles are tended toward the walls. In this figure the walls are shrunk and stretched with equal rates.

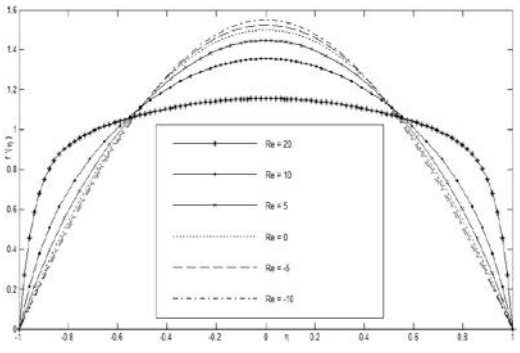

Fig. 3: $f'(\eta)$ is plotted against η for $\alpha_1 = 0 = \alpha_2$, $d = -1$ and different Re.

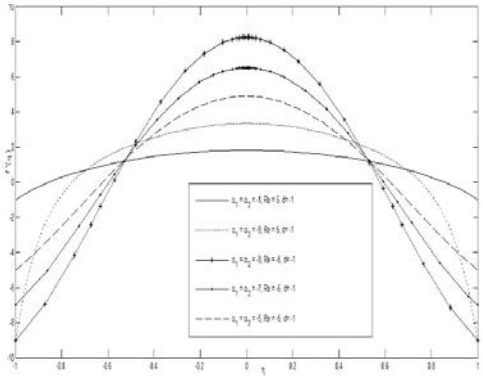

Fig. 4: $f'(\eta)$ is plotted against η for $\alpha_1 = \alpha_2 < 0$, $d = -1$ suction (injection).

In Fig. 5, f' is plotted against η for equal suction and injection at both walls. Both the walls are stretched with unit rates. In the current figure solid and dotted lines are representing injection and suction cases respectively. All the profiles are symmetrical about $\eta = 0$. For $\alpha_1 = \alpha_2 = 1$ and $d = -1$, we obtained straight velocity profiles. These profiles are equal to a constant $\alpha_1 = \alpha_2 = 1$ and do not depend on Re. In other words, for this choice of parameters values the flow is independent of Re. This means that, for equally stretched walls with unity, whenever fluids enter (leave) through the walls with equal rates, the flow in channel remain constant ($f'(\eta) = 1$) axially. No changes in the pattern of f' (for $\alpha_1 = \alpha_2 = 1$, $d = -1$) are observed for different values of Re. Back flow is observed for all other values except $\alpha_1 = \alpha_2 = 1$ $d = -1$. Back overflow is noted for large injection. Further, for these values of Re, f' is increased near the walls and decreasingly moved towards the centre. For suction, f' is uniformly decreased. In Fig. 6 effects of different d are observed on f'. For $d = 1$ and $\alpha_1 = \alpha_2 = 0$ the profile is linear and equal to zero everywhere in the domain. The solution for this set of parameters values (independent of Re) is trivial and confirmed by the numerical and perturbation methods. For $d = -1$, we got symmetrical profile about the centre line. For $d > 1$ reverse flow phenomena is observed. Back flow is dominant near the bottom wall and weak in the surrounding the wall. For increasing d, back overflow is observed. As d decreases from -1 to -5, the velocity profiles increase. For these choices of d the axial velocity of the fluid is high near the top plate as compared to the lower plate. For $d = 1$, flow is purely one dimensional and the velocity is equal to a constant. The normal velocity is equal to 1 and axial velocity is zero.

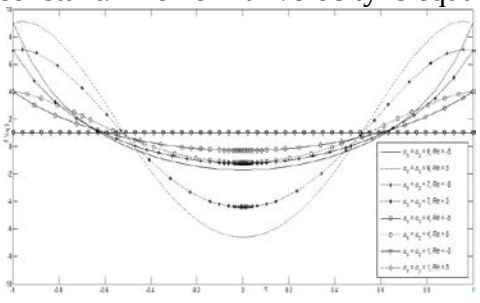

Fig. 5: $f'(\eta)$ is plotted against η for $\alpha_1 = \alpha_2$, $d = -1$ and suction (injection).

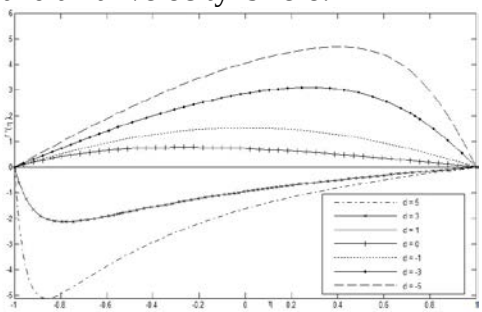

Fig. 6: $f'(\eta)$ is plotted against η for Re $= -5$, $\alpha_1 = \alpha_2 < 0$ and different values of d.

Effects of different d are found on f' against η in Fig. 7. In this figure, we obtained two families of graphs. One family of profiles is above the constant

profile ($f'=0$) and the other one is bellow it. The profiles corresponding to $d=0.7$ and $d=1.3$ are the mirror image of each other. Similar observations are noted for other value of d and the results are shown in Fig. 7. In this figure the profiles are decreasing with the increasing value of d in the limit $0\prec d\prec 1$. In addition, the two families of profiles are tending to a constant profile when d is approaching either from 0.1 to 1 or from 2 to 1. Effects of different $\alpha_1(\alpha_2)$ on f' (for equal injection at both walls) are observed. The lower (upper) wall is assumed fix. At the upper (lower) half of the channel f' is uniformly decreased as the values of $\alpha_1(\alpha_2)$ are increased from -5 to 5. The values of f' shot the upper (lower) plate according to the values of $\alpha_1(\alpha_2)$. Effects of different $\alpha_1(\alpha_2)$ on f' is observed for equal suction at both walls and upper (lower) plate is fixed. f' is decreased at upper (lower) half of the channel with the values of $\alpha_2(\alpha_1)$ when increased from -5 to 5. Further, f' met the values of $\alpha_2(\alpha_1)$ at the lower (upper) wall. f' is increased at the lower (upper) half of the channel with the increase of $\alpha_2(\alpha_1)$ when $\alpha_2(\alpha_1)$ changed from -5 to 5.

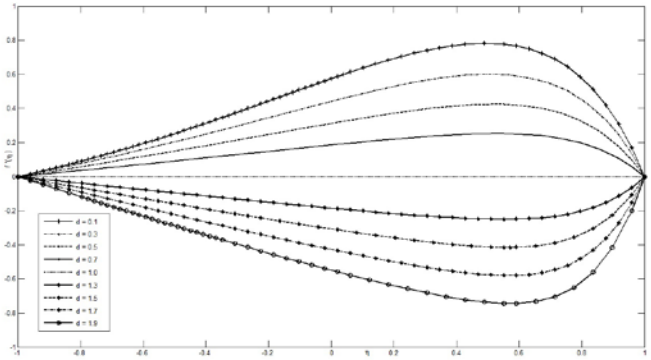

Fig. 7: $f'(\eta)$ is plotted against η for Re = –5, $\alpha_1 = \alpha_2 = 0$ and different positive values of d.

For $\alpha_1=\alpha_2=1$ and $d=-1$, we obtained a constant f'. This exact solution ($f=\eta$) is confirmed by perturbation and numerical methods. This means that both walls are stretched with equal rates of unity and equal suction or injection in top and bottom walls is taken into account. In Table 1 the perturbation solution is compared with the numerical solution for different values of parameters. For small values of parameters the two solutions are exactly matched. In this table those values of f are calculated for which we have noted some difference between the two solutions. The two solutions are exactly the same up to the four decimal places at all points except a few points between walls and the core of the channel. The asymptotic results are compared with numerical results for large and

small values of parameters respectively. For large values of the parameters the two results are equal. For moderate and small values of parameters, we obtained small errors between the two solutions at certain points. This error is shown in table and arises at the points between centre and walls. The two solutions are matched to the best accuracy level and the results are up to the mark. The non-dimensionalized shear stress $\bar{\tau} = \tau / \tau_w = f''(\eta)$ is obtained from Eq. (11) and $f(\eta)$ may be obtained from Eqs. (8, 9) by the methods in hand. The mean pressure is obtained from Eq. (10) and has the form:

$$p(x,\eta) = \frac{1}{2}[\, p(x_0,1) + p(x_0,-1) + \frac{\mu v_w}{4h^3}(x^2 - x_0^2)$$

$$-\frac{\rho v_w^2}{4}\{-\frac{1}{2}(1-d)^2(1-\eta) + (1-d^2)\eta^2\}].$$

The above expression is quadratic in η and will not vary against η for $d = 1$. The exact solution is independent of Re and the stress will be zero in this case.

5. Conclusion

The paper is concluded with the remarks that the compatibility of the different solutions is checked and responses of flow properties to the different parameters by using these solutions are accurately found and calculated. Excellent agreement between the perturbation and numerical solutions for $f(\eta)$ was found. Whereas the asymptotic solution was compared with the numerical solution for large values of the parameters and the two results are matched to best accuracy level. Moreover, the asymptotic results were also matched with numerical results for small values of parameters in Table 1 and good agreement between the two is found. Straight axial velocity profiles were obtained for a set of parameters value ($\alpha_1 = \alpha_2$ and $2\alpha_1 + d = 1$) and equal to constants ($\alpha_1 = \alpha_2$). These solutions include a trivial axial profile (exact solution) for $\alpha_1 = \alpha_2 = 0$ and $d = 1$. In all these cases, the flow is independent of Re when these special values are chosen. These are exact solutions of the Navier-Stokes equations. These exact solutions are verified by the numerical and perturbation methods. For $d = -1$, $\alpha_2 = 0(\alpha_1 = 0)$, fixed values of Re and different values of $\alpha_1(\alpha_2)$, the profiles of f' were scaled on $\eta = 1(-1)$ according to the values of $\alpha_1(\alpha_2)$. All other changes in the profiles corresponding to these two sets of parameters values were common. Three different solutions were obtained for a single set of parameters values. The results of [3] were recovered for the special values $A = B = 0$ and $v_w = -u_w$, or, equivalently, $d = -1$ and $\alpha_1 = \alpha_2 = 0$.

REFERENCES

[1] *B. C. Sakiadis*, Boundary-layer behavior on continuous solid surfaces: I. Boundary-layer equations for two-dimensional and axisymmetric flow, J. AIChE., 7 (1961), 26-28.

[2] W. H. H. Bank, Similarity solutions of the boundary-layer equations for a stretching wall, J. Mec. Theor. Appl., **2** (1983), 375-392.

[3] *A. S. Berman*, Laminar flow in channels with porous walls, J. Appl. Phys., **24** (1953), 1232-1235.

[4] *J. R. Sellars*, Laminar flow in channels with porous walls at high suction Reynolds numbers, J. Appl. Phys., **26** (1955), 489-490.

[5] *S. M. Cox, J. R. King*, On the asymptotic solution of a high order non-linear ordinary differential equations, Proc. R. Soc. London A, **453** (1997), 711-728.

[6] *N. M. Bujurke, V. S. Madalli, B. G. Mulimanib*, Long series analysis of laminar flow through parallel and uniformly porous walls of different permeability, Comput. Methods Appl. Mech. Engng.., **160** (1998), 39-56.

[7] *L. Zheng, N. Zhao, X. Zhang*, Asymptotic solutions for laminar flow in a channel with uniformly accelerating rigid porous walls, J. UST Beijing, **14** (2007), 405-409.

[8] *J. Majdalani, Z. Chong, A. D. Christopher*, Two-dimensional viscous flow between slowly expanding or contracting walls with permeability, J. Biomechanics, **35** (2002), 1399-1403.

[9] *E. Rahimi, A. Rahimifar, R. Mohammadyari, I. Rahimipetroudi, M. Rahimi-Esbo*, Analytical approach for solving two-dimensional laminar viscous flow between slowly expanding and contracting walls, Ain Shams Eng. J., **7** (2016), 1089-1097.

[10] *B. K. Jha, B. Aina*, Role of suction/injection on steady fully developed mixed convection flow in a vertical parallel plate microchannel. Ain Shams Eng. J., (accepted).

[11] *G. Huang, Y. Zhu, L. Zhiyuan, X. L. Ouyang, P. X. Jiang*, Experimental investigation of transpiration cooling with phase change for sintered porous plates, Int. J. Heat Mass Trans., **114** (2017), 1201-1213.

[12] *A. R. Hassan, R. Maritz, J. A. Gbadeyan*, A reactive hydromagnetic heat generating fluid flow with thermal radiation within porous channel with symmetric convective cooling, Int. J. Therm. Sci., **122** (2017), 248-256.

[13] *M. M. Rashidi, M. Reza, S. Gupta*, MHD stagnation point flow of micropolar nanofluid between parallel porous plates with uniform blowing, Powder Tech., **301** (2016), 876-885.

[14] *H. Mirgolbabaee, S. T. Ledari, D. D. Ganji*, Semi-analytical investigation on micropolar fluid flow and heat transfer in a permeable channel using AGM, J. Assoc. Arab Univ. Basic Appl. Sci., (accepted).

[15] *T. Cebeci, H. B. Keller*, Shooting and parallel shooting methods for solving the Falkner-Skan boundary-layer equation, J. Comp. Phys., **7** (1971), 289-300.